Textures and Microstructures, 1995, Vol. 24, pp. 43–52
Reprints available directly from the publisher
Photocopying permitted by license only

© 1995 OPA (Overseas Publishers Association)
Amsterdam B.V. Published under license by
Gordon and Breach Science Publishers SA
Printed in Malaysia

TEXTURE AND MICROSTRUCTURE DEVELOPMENT IN Al_2O_3-PLATELET REINFORCED Ce-ZrO_2/Al_2O_3 LAMINATES PRODUCED BY CENTRIFUGAL CONSOLIDATION

RYAN K. ROEDER, KEITH J. BOWMAN AND KEVIN P. TRUMBLE

School of Materials Engineering, Purdue University, West Lafayette, IN 47907

(Received 2 August 1994)

A dispersed, low-solids-fraction suspension containing Ce-ZrO_2, fine Al_2O_3 and 5 vol% Al_2O_3-platelets was segregated using centrifugal consolidation to produce functionally gradient laminates (FGLs). Platelet alignment facilitated efficient packing of highly anisometric platelets to high densities. The complexity and anisotropy of the microstructure warrants a quantitative analysis of the microstructural evolution prior to any property evaluation. Quantitative image analysis was used to examine changes in the volume fraction, dimensional anisotropy, and gradient of pores and platelets with sintering time. In all cases, special attention was given to the effects of texture during microstructural evolution. Platelet alignment enhanced densification via anisotropic shrinkage, overcoming constraint that otherwise inhibits densification in platelet-containing materials. Also, platelet alignment and microstructural design were used to initiate and control anisotropic grain growth. Platelet growth (at the expense of smaller particles of the same phase) during annealing promoted further phase segregation and produced higher platelet content composites consisting of larger platelets, without having to consolidate high contents of large platelets.

KEY WORDS: Anisotropy, grain growth, densification, composite, ceramic laminates, alumina, zirconia.

INTRODUCTION

Almost twenty years ago, Garvie, Hannink, and Pascoe (1975) were the first to credit transformation induced plasticity for the high toughness of zirconia containing alloys. In the last decade, research in the development of advanced structural ceramics has focused on the optimization of transformation induced plasticity in zirconia toughened ceramics. Recent work by Marshall *et al.* (1990, 1991) has shown that introducing large, non-transforming microstructural units (e.g. Al_2O_3 layers) into ceria-partially-stabilized zirconia (Ce-ZrO_2) can widen an otherwise elongated transformation zone ahead of the crack tip. Non-transforming Al_2O_3 layers force adjacent widening of the transformation zone, increasing crack tip shielding. This anisotropic microstructure makes possible large increases in fracture toughness (in Ce-ZrO_2, from ~5 to 17.5 MPa•$m^{1/2}$) and extensive *R*-curve behavior (Marshall, Ratto, Lange, 1991).

Extension of this Ce-ZrO_2/Al_2O_3 laminate concept to include Al_2O_3-platelets in non-transforming layers would result in several benefits. The higher strength of the Al_2O_3-platelets could induce further transformation zone widening. Also, platelets are known

to give rise to additional toughening mechanisms: platelet pull-out, crack deflection, crack bridging, and modulus load transfer (Evans, 1984; Heussner, Claussen, 1989; Chou, Green, 1993; Huang, Nicholson, 1993). The realization of these potential benefits depends on the orientation and location of the platelets within the already anisotropic layered microstructure. Thus, texture is critical to this proposed method of further toughness enhancement. Bowman and co-workers (Lee, Sandlin, Bowman, 1993; Sandlin, Peterson, Bowman, 1994, Sandlin, Bowman, 1994; Steinlage, *et al.*, 1994) have utilized texture quantification and optimization as a means for property enhancement in a variety of ceramics and ceramic composites. In all cases, the key to attaining optimized texture is found in microstructural design by manipulation of controllable processing routes. Intelligent use of this strategy results in orientation-selective processing (OSP) of materials.

In this study, the Ce-ZrO_2/Al_2O_3 laminate concept of Marshall *et al.* (1991) is extended to include Al_2O_3-platelets via a unique processing approach. Microstructural design is achieved through a combination of orientation-selective colloidal and thermal processing. Centrifugal consolidation applies large settling forces on particles, which segregate dispersed multi-component suspensions into gradient layers with aligned platelets. Further increases in anisotropy are also possible if platelets are located such that growth (at the expense of smaller Al_2O_3 particles) is facilitated during sintering. Quantitative image analysis is introduced as a means to analyze complex and anisotropic functionally gradient laminate (FGL) microstructures. Pore, platelet, and gradient layer evolution is examined with sintering time, paying special attention to the effects of texture during microstructure evolution.

EXPERIMENTAL PROCEDURE

Colloidal Processing

An aqueous suspension containing 8 vol% solids (Table 1) at pH = 3 (using HNO_3) was dispersed by ultrasonication (Sonicator^R W-380, Heat Systems-Ultrasonics Inc., Farmingdale, NY). This ternary Ce-ZrO_2/Al_2O_3/Al_2O_3-platelet suspension was centrifugally consolidated. Molds placed within the four swinging buckets of a centrifuge (model CL, Damon/IEC, Needham Hts., MA) consisted of polyethylene tubes (2.5 cm inner diameter) with a balloon stretched and fastened over one end. Prior to suspension addition, 4 ml of de-ionized water at pH = 3 (using HNO_3) was placed in each of the four molds to facilitate packing layers of uniform thickness. The suspension was consolidated by centrifuging 40 sequential suspension additions (in each mold) of 0.25 ml at ~2150 g for 2 min per addition (Figure 1). Since this procedure required 1.5–2 h, care was taken to maintain the bulk suspension at pH = 3 under constant mixing. At the completion of consolidation, the supernatants were poured off, yielding tabular green bodies within their molds.

Thermal Processing

Dried green bodies were fired at 1200°C (400°C/hr. ramp) for 1 h. This light sintering provided sufficient strength for sectioning, while adding minimal densification for examining the near-green microstructure. Fired bodies were sectioned with a diamond saw into rectangular prisms (~1.3 × 8 × .35 cm) which were annealed at 1600°C (800°C/hr. ramp) for 1 min and 1, 4, 8, 16, 32, and 64 h, followed by furnace cooling.

Table 1 Starting Powders and Data.

Powder	*Percent of Solids (vol%)*	*Density (g/cc)*	*Average Particle Size (μm)*	*Trade Name/Supplier*
Al_2O_3-platelets	5.0	3.98*	1–25*#	Elf Atochem, Paris, France
fine Al_2O_3	47.5	3.98*	0.2*#	AKP-50; Sumitomo Chemical, New York, NY
fractionated Ce-ZrO_2	47.5	6.20*	2.6#	TZ-12Ce; Tosoh Ceramics Div., New Milford, CT

* from manufacturers data
# measured using a Coulter® LS130 (with fluid module) particle size analyzer

Evaluation

The density and dimensions of all specimens were measured after drying, firing, and subsequent annealing. The density of the dried green specimens was estimated by massing and measuring their dimensions. Once fired and annealed, the density was measured using Archimedes' principle. Measured dimensions also allowed for the calculation of linear and volume shrinkages.

All microscopy specimens were prepared by polishing manually with 45, 30 and 15 μm diamond paste on glass, followed by 6 μm, 3 μm, 1 μm, and .25 μm diamond paste on polishing cloths (Texmet®, Buehler, Lake Bluff, IL) using an automatic polisher (Minimet®, Buehler). All specimens were thermally etched in air for 6 min at 1550°C, and sputter coated with platinum. The microstructure was examined using a scanning electron microscope (JEOL JSM-35CF, Tokyo, Japan), taking advantage of high phase contrast due to the large difference in atomic number between Al and Zr.

SEM micrographs of single layers of functionally gradient laminates (FGLs) were entered into a commercially available image analysis system (Integrated Microanalyzer of Imaging and X-Ray, Princeton Gamma-Tech (PGT), Inc., Princeton, NJ). Binary images were created for each anneal time to feature pores, Al_2O_3, and Al_2O_3-platelets. In enhanced pore images, all visible pores were isolated utilizing charging contrast around pore edges in SEM images. However, the extent of charging prevented generation of a suitable porosity image for the more porous 1 min anneal time. The lack of mutual solubility of Al_2O_3 and Ce-ZrO_2, and the absence of any intermediate phases, precludes any significant changes in overall phase content during heat treatment. Therefore, the enhanced Al_2O_3 images were prepared by adjusting the area fraction of Al_2O_3 in one layer to match the amount known to be present (calculated considering the sample porosity and Al_2O_3 fraction in the suspension). Finally, the enhanced Al_2O_3-platelet images were created by isolating all visible platelets from the Al_2O_3 images. Thus, all computer enhanced images were created systematically, allowing comparison between different anneal times.

The PGT software provides geometrical data about each feature, allowing a quantitative description of microstructural evolution. For both pores and platelets, this description includes changes in the feature volume fraction, dimensional anisotropy, and distribution across the gradient layer. Feature volume fractions were determined by measuring the area fraction within regions of one layer thickness. Quantification of dimensional anisotropy was made possible by measuring feature dimensions projected

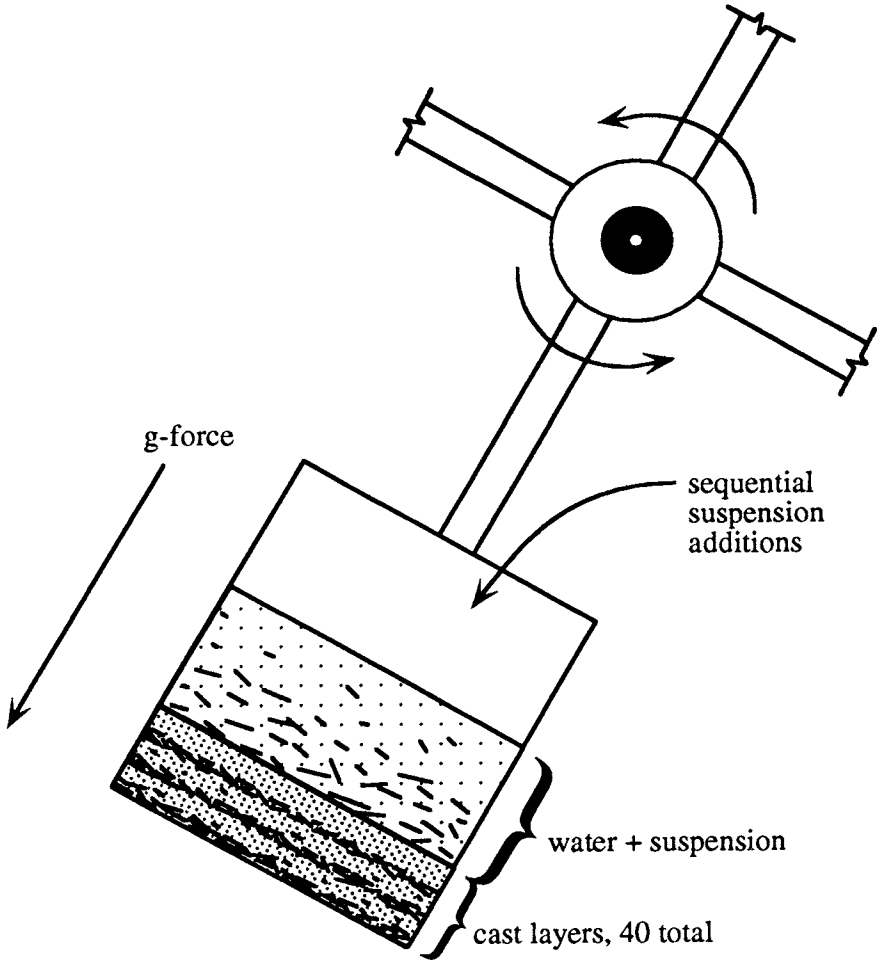

Figure 1 Schematic representation of centrifugal consolidation of functionally gradient layers in the swinging bucket of a centrifuge.

on the x (parallel to layers) and y (perpendicular to layers) axes, called "ferets" (Princeton Gamma-Tech, 1993). Feature distribution in gradient layers was obtained by measuring feature area (or area fraction) in successive narrow boxes placed across a layer.

RESULTS AND DISCUSSION

Consolidation Behavior

The consolidation behavior of the ternary suspension is revealed in the microstructure of a single layer after a short anneal time (Figure 2a). The combination of high intertial g-forces and a dispersed, low solids content suspension promoted segregation (due to differential settling rates) of suspension components by density and size (see Table 1).

The large Al_2O_3-platelets were the first to settle out of suspension additions, followed by the more dense, but much smaller, Ce-ZrO_2 particles and finally the fine Al_2O_3. As is evident, centrifugal consolidation uniquely produces highly controlled microstructures through control of the *g*-forces on particles, constituent particle size, constituent density, suspension viscosity, and interparticle surface forces. With proper consideration of the first three variables, segregation can even be prevented in a low solids content, dispersed suspension containing components of greatly differing density and particle size (Roeder, Bowman, Trumble, 1994).

High particle packing densities were achieved despite the presence of anisometric platelets. Density of green bodies averaged 59% of theoretical density. The key to attaining these high particle packing densities lies in efficient particle packing via platelet alignment. Several factors contributed to efficient particle packing: high *g*-forces on particles, repulsive interparticle potentials, low solids content, and segregation.

A prior example of a ceramic/ceramic FGL with a constantly varying phase gradient is apparently non-existent in literature. Multi-layered laminates with homogeneous layers of alternating (Marshall, Ratto, Lange, 1991) and sequentially changing (Moya, *et al.*, 1992) phase content have been produced. Examples of constantly varying phase gradient in metal-matrix composites (MMCs) do exist, though not in laminates. In one example (Fukui, 1991), a centrifugal melt casting technique has utilized segregation to produce a constantly varying gradient of ceramic inclusions in a metal matrix.

Densification and Pore Evolution

Densification of the FGL layers with increasing anneal time is displayed pictorially by computer-enhanced images of pores (Figure 2d–f) and quantitatively by plots of the pore fraction (Figure 3a). Post-annealed relative densities reached as high as 99.5% (by Archimedes' measurement) despite the presence of matrix-constraining platelets and the use of pressureless sintering. Furthermore, linear shrinkages (by measuring FGL dimensional changes) averaged 15% parallel to the layers and 20% orthogonal to the layers, making shrinkage 33% greater perpendicular to the layers. Thus, platelet alignment limited constraint to directions within the plane of layers and platelets, such that densification occurred primarily perpendicular to layers and platelets.

Evolution of the pore gradient with anneal time is shown pictorially by computer images of enhanced pores (Figure 2d–f) and quantitatively by plots of the pore area distribution across a layer (Figure 3c). At short (up to 4 h) anneal times, pores were concentrated in platelet-containing regions. These pores resulted from less efficient particle packing in the platelet regions and were accordingly located between basal faces of the platelets. The ratio of pore dimensions projected on the *x*- and *y*- axes (essentially an aspect ratio relegated to the directions of interest) reveal that the oriented platelets induced a preferred orientation in pores at these short anneal times (Figure 3b). The pore concentration in platelet regions and the dimensional anisotropy of pores both decreased with longer anneal times and virtually disappeared by 32 and 8 h, respectively (Figure 3b and c).

Additionally, data from image analysis suggests that at long anneal times (over 4 h) pores appear and grow in the non-platelet-containing regions of layers, where almost no pores were initially present at short anneal times (Figures 2d–f and 3c). However, at the micrograph magnifications necessitated by platelet size and layer thickness, many pores were too small to be resolved and enhanced for image analysis. Comparison of the pore fractions measured by Archimedes' principle and image analysis (area

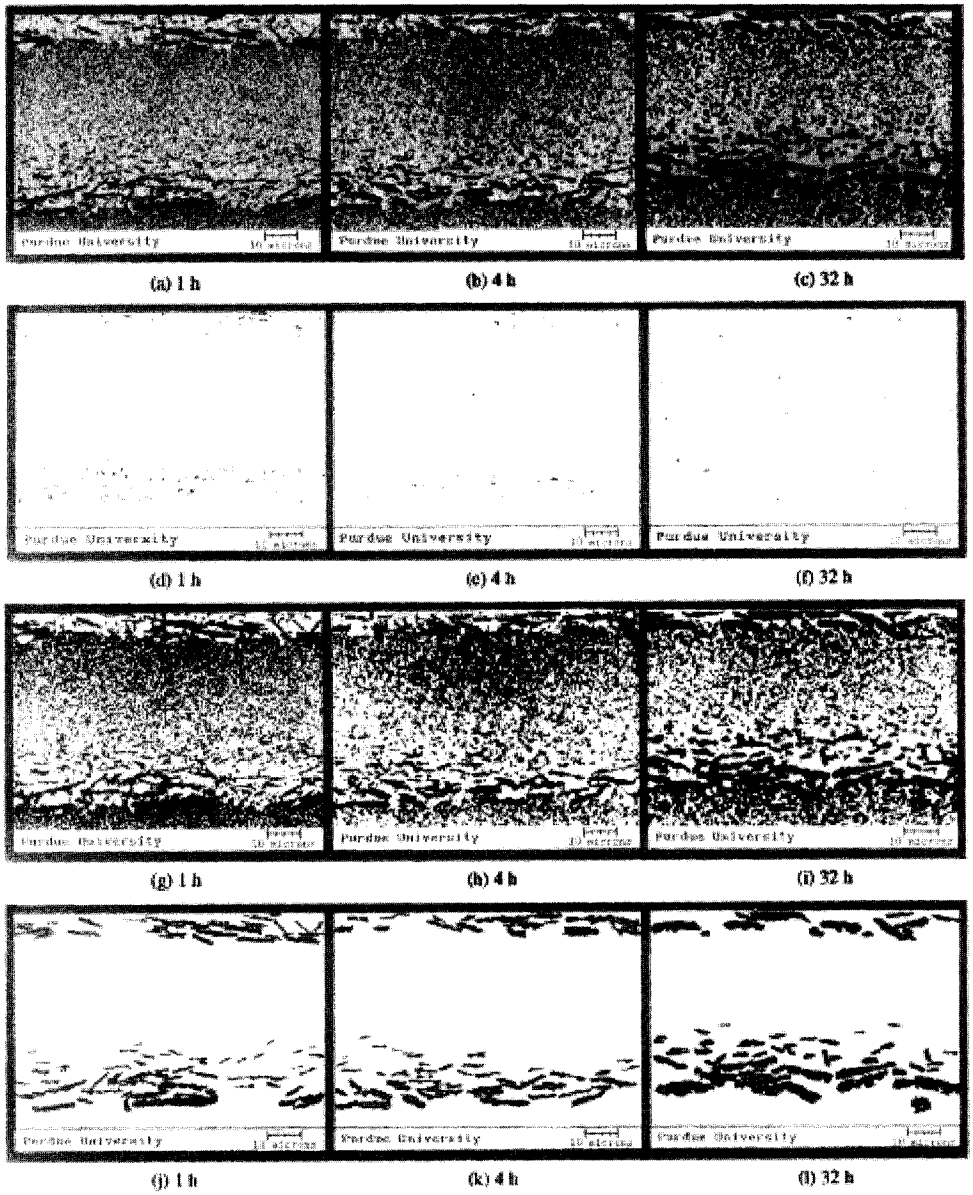

Figure 2 SEM micrographs of FGL single layers at selected anneal times (a–c) with corresponding computer images showing enhanced (black) porosity (d–f), Al_2O_3 (g–i), and Al_2O_3-platelets (j–l).

fraction of single layers assumed to be equal to that of the FGL) reveal that image analysis did consistently underestimate the pore fraction (Figure 3a). Thus, pores too small to be resolved for image analysis grew into larger pores that could be resolved. The reasons for this apparent pore growth (or desintering) might include any or all

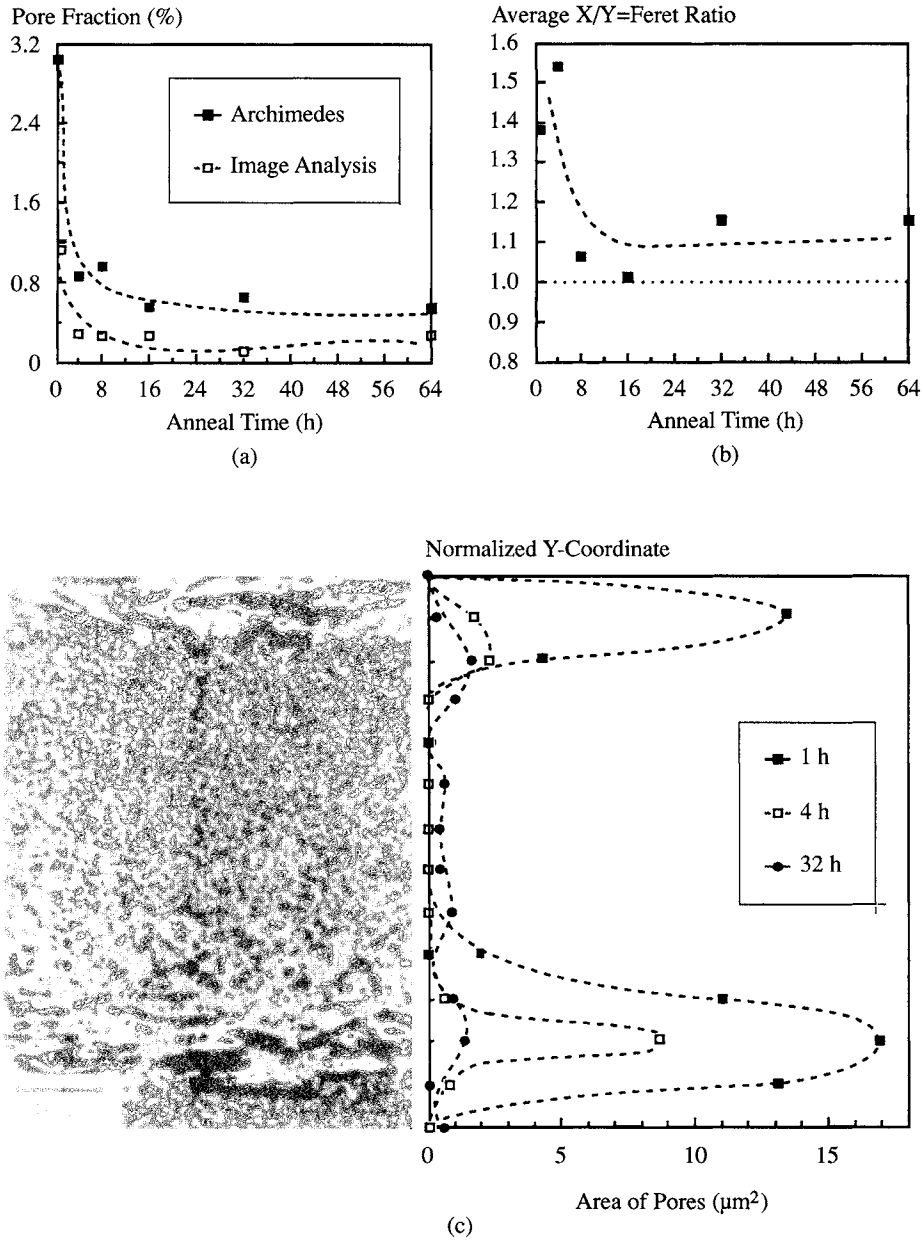

Figure 3 Porosity evolution with anneal time showing changes in (a) the pore fraction, (b) the ratio of pore dimensions projected on the x–y axes, and (c) the gradient of pore area across a single layer (microstructure for the 4 h anneal time is shown on left).

of the following issues: constrained densification, pore coalescence during grain growth, and pore coordination (Zhao, Harmer, 1988; Kellet, Lange, 1989; Slamovich, Lange, 1992; Sudre, *et al.*, 1992; Sudre, Lange, 1992).

Al_2O_3-Platelet Evolution

Growth of Al_2O_3-platelets in FGL layers with increasing anneal time is shown pictorially by computer-enhanced images of platelets (Figure 2j–l) and quantitatively by plots of the platelet area fraction (Figure 4a). Recalling that Al_2O_3 and Ce-ZrO_2 are mutually insoluble and exhibit no intermediate phases, the increasing platelet area fraction is evidence that the large platelets grew at the expense of the finer Al_2O_3 particles. Since the average orientation angle of the platelets remained relatively constant for different heat treatments, the volume of the oriented phase increased approximately four times (from 5 to ~20 vol%). Essentially, a 5 vol% platelet composite became a ~20 vol% platelet composite via grain growth. Implications for making higher platelet content composites consisting of larger platelets without having to consolidate high contents of large platelets could be significant.

Evolution of the Al_2O_3/Al_2O_3-platelet gradient with annealing is shown in computer-enhanced images of Al_2O_3 (Figure 2g–i) and quantitatively by plots of the Al_2O_3 area fraction distribution across a layer (Figure 4c). As the anneal time is increased, the Al_2O_3 fraction increases in the platelet-containing region and decreases in the region that initially had a high content of fine Al_2O_3. Notice that at early anneal times the ends (top and bottom) of the area fraction distribution do not match (Figure 4c), indicative of the discontinuity between layers. However, as the anneal time increases the ends approach and remain relatively constant (though not shown, at the 8–64 h anneal times all layers had similar Al_2O_3 area fraction distributions). Thus, platelet growth is facilitated by a migration of Al_2O_3 across the gradient layer to platelets. If a gradient layer had a similar phase gradient but a uniform grain size gradient, the observed phase redistribution would still be expected, though to a lesser extent.

Al_2O_3 preferentially grew perpendicular to FGL layers on platelet basal planes (Figures 4b and 2j–l). The measured anisotropic platelet growth is a result of two factors. First, many platelets are in direct contact with the fine Al_2O_3 particles of the previous layer, providing a large source of consumable grains. Second, microstructural constraint contributes to platelet growth anisotropy. Since platelets generally lie end-to-end, there is little room for growth to occur before many platelets are in lateral contact with one another. Consequently, the unconstrained densification perpendicular to layers and platelets is faster, reaching the grain growth regime earlier during sintering. Thus, platelet alignment and microstructure design can be used to initiate and control anisotropic grain growth.

SUMMARY

1. The Ce-ZrO_2/Al_2O_3 laminate concept was extended to include Al_2O_3-platelets, facilitating increased anisotropy through a combination of orientation-selective colloidal and thermal processing.
2. Functionally gradient laminates were produced by segregating dispersed suspensions, while consolidating highly anisometric platelets to high packing densities via platelet alignment.
3. Platelet alignment resulted in anisotropic shrinkage, overcoming constraint that otherwise inhibits densification in platelet-containing materials.
4. Platelet growth (at the expense of smaller particles of the same phase) produced higher platelet content composites consisting of larger platelets, without having to consolidate high contents of large platelets.

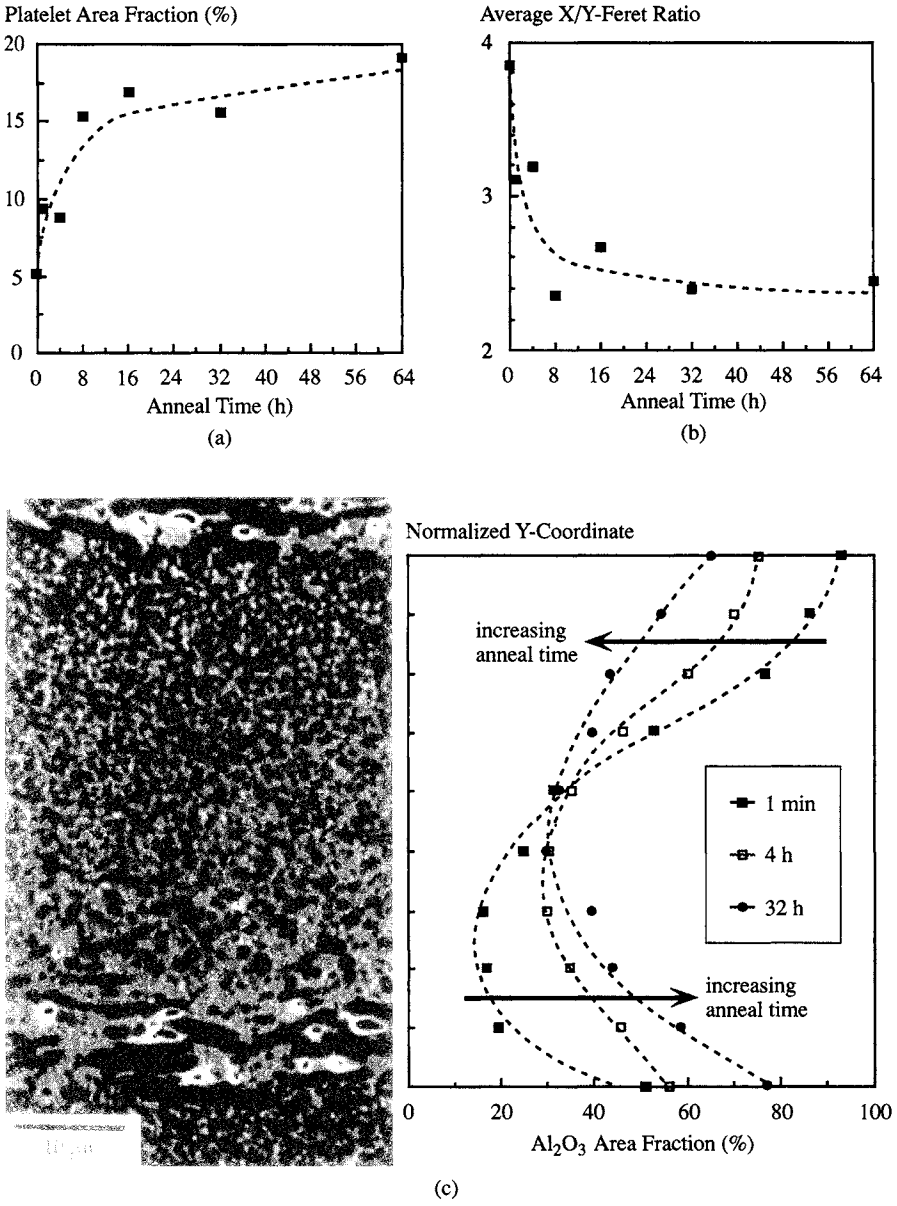

Figure 4 Al_2O_3-platelet evolution with anneal time showing changes in (a) the platelet area fraction, (b) the ratio of platelet dimensions projected on the x–y axes, and (c) the gradient of Al_2O_3 across a single layer (shown for the 4 h anneal time matching the normalized y-coordinate).

5. Grain growth induced segregation of Al_2O_3 resulted in phase redistribution enhanced by the presence of large size gradient due to the platelets.
6. Platelet alignment and microstructural design can be used to initiate and control anisotropic grain growth.

Acknowledgements

The authors thank B. Jarosinski (Praxair Surface Technologies, Indianapolis, IN) for particle size measurements, and J. Blendell (NIST) for providing the Atochem Al_2O_3-platelets. This research was supported by the National Science Foundation through grants DMR-91-21948 and DMR-93-57496.

References

1. Chou, Y. and Green, D. J. (1993). Silicon Carbide Platelet/Alumina Composites: III, Toughening Mechanisms. *J. Am. Ceram. Soc.,* **76**(8), 1985–1992.
2. Evans, A. G. (1984). Toughening Mechanisms in Zirconia Alloys. In *Science and Technology of Zirconia II,* edited by Claussen, M., Ruhle, M. and Heuer, A. H., pp. 193–212. Columbus: American Ceramic Society.
3. Fukui, Y. (1991). Fundamental Investigation of Functionally Gradient Material Manufacturing System using Centrifugal Force. *JSME Int'l Journal,* Series III, **34**(1), 144–148.
4. Garvie, R. C., Hannink, R. H. and Pascoe, R. T. (1975). Ceramic Steel. *Nature (London),* **258**(5537), 703–704.
5. Heussner, K. and Claussen, N. (1989). Yttria- and Ceria-Stabilized Tetragonal Zirconia Polycrystals (Y-TZP, Ce-TZP) Reinforced with Al_2O_3 Platelets. *J. Eur. Ceram. Soc.,* **5**, 193–200.
6. Huang, X. and Nicholson, P. S. (1993). Mechanical Properties and Fracture Toughness of α-Al_2O_3-Platelet-Reinforced Y-PSZ Composites at Room and High Temperatures. *J. Am. Ceram. Soc.,* **76**(5), 1294–1301.
7. Kellet, B. J. and Lange, F. F. (1989). Thermodynamics of Densification: I, Sintering of Simple Particle Arrays, Equilibrium Configurations, Pore Stability, and Shrinkage. *J. Am. Ceram. Soc.,* **72**(5), 725–734.
8. Lee, F., Sandlin, M. S. and Bowman, K. J. (1993). Toughness Anisotropy in Textured Ceramics. *J. Am. Ceram. Soc.,* **76**(7), 1793–1800.
9. Marshall, D. B. (1990). Crack Shielding in Ceria-Partially Stabilized Zirconia. *J. Amer. Ceram. Soc.,* **73**(10), 3119–3121.
10. Marshall, D. B., Ratto, J. J. and Lange, F. F. (1991). Enhanced Fracture Toughness in Layered Microcomposites of Ce-ZrO_2 and Al_2O_3. *J. Am. Ceram. Soc.,* **74**(12), 2979–2987.
11. Moya, J. S., Sanchez-Herencia, A. J., Requena, J. and Moreno, R. (1992). Functionally Gradient Ceramics by Sequential Slip Casting. *Materials Letters,* **14**, 333–335.
12. Princeton Gamma-Tech (PGT), Inc. (1993). *Integrated Microanalyzer for Imaging and X-Ray (IMIX) Software Manual,* version 7, edited by Kuszewski, M. L., Princeton, NY: Princeton Gamma-Tech, Inc..
13. Roeder, R. K., Bowman, K. J. and Trumble, K. P. (1994). Unpublished results.
14. Sandlin, M. S., Peterson, C. R. and Bowman, K. J. (1994). Texture Measurement by Stereological Analysis of Microstructures Containing Plates. *J. Am. Ceram. Soc.,* **77**(8), 2127–2131.
15. Sandlin, M. S. and Bowman, K. J. (1994). Texture Development in AlN-SiC Platelet Composites. *J. Am. Ceram. Soc.,* submitted May 1994.
16. Slamovich, E. B. and Lange, F. F. (1992). Densification of Large Pores: I, Experiments. *J. Am. Ceram. Soc.,* **75**(9), 2498–2508.
17. Steinlage, G., Roeder, R., Trumble, K., Bowman, K., Li, S. and McElresh, M. (1994). Preferred Orientation of BSCCO via Centrifugal Slip Casting. *J. Materials Research,* **9**(4), 833–836.
18. Sudre, O., Bao, G., Fan, B. Lange, F. F. and Evans, A. G. (1992). Effect of Inclusions on Densification: II, Numerical Model. *J. Am. Ceram. Soc.,* **75**(3), 525–531.
19. Sudre, O. and Lange, F. F. (1992). The Effect of Inclusions on Densification: III, The Desintering Phenomenon. *J. Am. Ceram. Soc.,* **75**(12), 3241–3251.
20. Zhao, J. and Harmer, M. P. (1988). Effect of Pore Distribution on Microstructural Development: II, First and Second Generation Pores. *J. Am. Ceram. Soc.,* **71**(7), 530–539.